

Laser wakefield acceleration by petawatt ultra-short laser pulses

L. M. Gorbunov*

P. N. Lebedev Physics Institute, Russian Academy of Sciences, Leninskii prospect 53, Moscow 119991, Russia

S. Yu. Kalmykov

*The Department of Physics and Institute for Fusion Studies,
The University of Texas at Austin, One University Station C1500, Austin, Texas 78712 and
Centre de Physique Théorique (UMR 7644 du CNRS), École Polytechnique, 91128 Palaiseau, France*

P. Mora

*Centre de Physique Théorique (UMR 7644 du CNRS), École Polytechnique, 91128 Palaiseau, France
(Dated: October 29, 2018)*

An ultra-short (about 30 fs) petawatt laser pulse focused with a wide focal spot (about 100 μm) in a rarefied plasma ($n_0 \sim 10^{17} \text{cm}^{-3}$) excites a nonlinear plasma wakefield which can accelerate injected electrons up to the GeV energy without any pulse channelling. In these conditions, propagation of the laser pulse with an over-critical power for relativistic self-focusing is almost the same as in vacuum. The nonlinear quasi-plane wake plasma wave, whose amplitude and phase velocity vary along the laser path, effectively traps and accelerates injected electrons with a wide range of initial energies. Electrons accelerated along two Rayleigh lengths (about eight centimeters) can gain an energy up to 1 GeV. In particular, the electrons trapped from quite a long ($\tau_b \sim 330$ fs) non-resonant electron beamlet of 1 MeV particles eventually form a low emittance bunch with energies in the range 900 ± 50 MeV. All these conclusions follow from two-dimensional simulations performed in cylindrical geometry by means of the fully relativistic time-averaged particle code WAKE.

PACS numbers: 52.35 Mw, 52.38 Hb, 52.38 Kd

I. INTRODUCTION

In the original, or "standard", scheme of laser wakefield acceleration (LWFA) [1, 2], a laser pulse of duration smaller than a period of plasma oscillation $\tau_p \equiv 2\pi/\omega_p$ excites a wake electron plasma wave (wakefield) with a phase velocity close to the speed of light [here and elsewhere, $\omega_p = (4\pi n_0 e^2/m)^{1/2}$ is the electron plasma frequency, n_0 is the electron plasma density, m and $-|e|$ are the electron mass at rest and charge]. When the electron density perturbation exceeds the background density, the accelerating electric field of the nonlinear wake can reach tens of GV/m, which is by three orders of magnitude higher than that can be achieved in the conventional accelerators without material breakdown. To excite such a wakefield, a short laser pulse of very high intensity is needed, that is, $I_0 \lambda_0^2 > 1.4 \times 10^{18} \text{ Wcm}^{-2} \mu\text{m}^2$ (where λ_0 is a laser wavelength). Reaching this range of intensities for lower laser energy in previous experiments [3] made necessary a tight beam focusing. The laser focal spot with a radius $r_0 \sim 10 \mu\text{m}$ gave a longitudinal extent of accelerating plasma (estimated as two Rayleigh lengths $2Z_R = 2\pi r_0^2/\lambda_0$) of the order of a few millimeters. Hence, the observed energy gain of electrons injected in the wake was moderate in spite of a high accelerating gradient. Also, very narrow plasma wake driven by a tightly focused laser is ineffective for trapping and acceleration of

injected electrons: the scale of radial variation was considerably smaller than the axial wavelength, and most of the electrons were expelled by strong radial electric fields. Only few electrons were trapped and accelerated in the three-dimensional potential wells [3].

The petawatt (10^{15} W) CPA lasers of new generation, which are under construction now [4], are capable of delivering ultra-short pulses (tens of femtoseconds) which can be focused with a relatively large focal spot ($r_0 \sim 100 \mu\text{m}$) yet having a relativistic intensity ($I_0 > 10^{18} \text{ W/cm}^2$) on axis. In this case, the effective acceleration distance (two Rayleigh lengths) is naturally elongated up to about ten centimeters, and the GeV energy range can be achieved by using the standard LWFA technique without external optical guiding [2]. In the scheme proposed, the plasma wavelength is smaller than the wake radial size. The large transverse extent of the wakefield structure reduces the detrimental effect of radial forces on accelerated electrons.

Anticipating this attractive chance to reach the GeV range of electron energy by using the standard LWFA, we analyze in this paper theoretically and numerically the details of laser pulse and wakefield evolution, and simulate the acceleration of an electron bunch in a wide range of parameters typical of those prospective experiments. The simulations have been carried out using the code WAKE [5, 6]. The laser parameters in the simulations are fixed: the laser wavelength $\lambda_0 = 0.8 \mu\text{m}$, the pulse energy 30 J, the pulse duration $\tau_L = 30$ fs, the radius of focal spot $r_0 = 100 \mu\text{m}$ (hence, the maximum intensity in vacuum is $I_0 \approx 6.4 \times 10^{18} \text{ W/cm}^2$). In the

*Electronic address: gorbun@sci.lebedev.ru

simulations of electron acceleration the electron density of unperturbed plasma is $n_0 = 1.12 \times 10^{17} \text{ cm}^3$, which gives the period of plasma oscillation $\tau_p \approx 330 \text{ fs}$ and the plasma wavelength $\lambda_p = 2\pi/k_p \approx 100 \text{ }\mu\text{m}$ (where $k_p = \omega_p/c$). Then, the normalized pulse duration and width are $\omega_p\tau_L = 0.56$ and $k_p r_0 = 6.28$, respectively. The relativistic factor corresponding to the laser group velocity $\gamma_g \equiv \omega_0/\omega_p = 125$. The laser power exceeds by a factor of four the critical power for the relativistic self-focusing $P_{cr} = 16.2(\omega_0/\omega_p)^2 \text{ GW}$ [7].

The paper is organized as follows. Numerical study of nonlinear effects in propagation of ultra-short petawatt laser pulse through rarefied plasma is given in Sec. II. The simulations supported by analytical considerations show that, for the parameters chosen, mutual cancellation of the relativistic and ponderomotive nonlinearities occurs in the pulse body. Thereby, only for very high intensities and/or electron densities (such that the critical power P_{cr} is exceeded by more than a factor of four) the nonlinearity produces some effect on the pulse shape.

Section III addresses the effect of laser pulse transverse evolution on the phase velocity of the two-dimensional (2D) nonlinear wakefield. In our framework, the effect originates from the relativistic nonlinearity of the plasma wake. The amplitude of the wakefield is proportional to the laser intensity which grows (drops) while the pulse focuses (diverges). On the other hand, the relativistic reduction in frequency is proportional, in the weakly relativistic approximation, to the wake amplitude squared. Therefore, as the pulse approaches the focal plane, the wake period stretches and its phase velocity drops below the pulse group velocity $v_g = c^2 k_0/\omega_0$. Beyond the focal plane the wake period shrinks and tends at infinity to the linear limit τ_p . At this stage, the wake phase accelerates and can become superluminal (i.e., exceeds not only the pulse group velocity in plasma but the vacuum speed of light). A similar effect was discussed previously for the case of longitudinally inhomogeneous plasmas [8]. Growth of the wake amplitude combined with the reduction in phase velocity provides conditions for highly efficient trapping of non-resonant injected electrons, $\gamma_{e0} \ll \gamma_g$, in the stage of laser focusing [here and below, $\gamma_{e0} \equiv (1 - v_{e0}^2/c^2)^{-1/2}$ is the initial Lorentz factor of the injected electrons corresponding to the velocity v_{e0} at the point of injection].

Wakefield acceleration of resonant electron bunches is considered in Sec. IV. Numerical simulations prove that the resonant conditions $\gamma_{e0} \approx \gamma_g$ or $\gamma_{e0} \approx \gamma_{p0}$ (where γ_{p0} is a relativistic factor given by the local phase velocity of wake at the point of electron injection) are beneficial for the ultra-short electron bunches only that are loaded directly in the accelerating and focusing quarter of the wake period ($\tau_p/4 \approx 80 \text{ fs}$ for the parameters given). Taking a longer bunch leads to a considerable energy spread because the resonant electrons injected at the bottom of the potential well stay there all the time and gain just a little energy. Injection of mono-energetic electron bunches with $\gamma_{e0} = \gamma_g = 125$ or $\gamma_{e0} = 42$ in the second period of

wakefield gives very similar output: after two Rayleigh lengths (about eight centimeters) the trapped electrons possess a broad energy spectrum (about 100% spread) with maxima at 0.5 GeV (for $\gamma_{e0} = 125$) or 0.75 GeV (for $\gamma_{e0} = 42$) and a cutoff at approximately 1 GeV. Tuning the energy of injected electrons to the resonance with a given period of wakefield reduces the final rms emittance of the accelerated electron bunch but has no effect on the final energy spread.

Acceleration of electron bunches injected with energies far below resonant is discussed in Sec. V. Simulations show that the electrons with initial energies 5 MeV and 1 MeV are not only effectively trapped and accelerated up to 1 GeV, but also reveal substantially less energy spread and lower root-mean-square (rms) emittance than in the resonant case discussed in Sec. IV. The slow electrons ($\gamma_{e0} = 0.08\gamma_g$ and $\gamma_{e0} = 0.016\gamma_g$) loaded near the bottom of the 2D potential well slip into the accelerating and focusing phase of the wake period and get effectively accelerated. In particular, acceleration of the 1 MeV electrons along twice the Rayleigh length produces a group of electrons with the energy $900 \pm 50 \text{ MeV}$ and rms emittance less than 10^{-4} mm mrad .

Section VI discusses and summarizes the results obtained. In Appendix A the analytical considerations are given of those nonlinear phenomena which have an effect on the propagation of ultra-short laser pulses in plasmas. The features of the plasma wakefield generated by diffracting Gaussian short laser beam are considered in Appendix B.

II. SHORT LASER PULSE PROPAGATION IN TENUOUS PLASMA: COMPENSATION OF RELATIVISTIC AND PONDEROMOTIVE NONLINEARITIES

Relativistic and ponderomotive nonlinearities of a short ($\omega_p\tau_L < 1$) and broad ($k_p r_0 > 1$) over-critical laser pulse ($P > P_{cr}$) partly cancel each other [9]. The vacuum-like propagation of such pulse [10], however, is not immune to the residual effect of the non-compensated relativistic nonlinearity (see Appendix A). We simulate the laser propagation, plasma wakefield excitation, and acceleration of injected test electrons by means of the 2D axially symmetric fully relativistic time-averaged particle code WAKE [5, 6], which is based on the quasi-static [9] and extended paraxial [11] approximations. The normalized slowly varying amplitude (envelope) of laser vector potential $a(\xi, r, z)$ is evaluated as a function of radial (r) and longitudinal (z) space variables and the retarded time $\xi/c = t - z/c$. In the simulation, the pulse propagates from the left to the right through a plasma slab centered at the vacuum focal plane $z = 0$. Simulation starts at a plane $z = z_0 < 0$ and terminates at a symmetric plane $z = |z_0|$. Initial laser beam with the parameters listed in Introduction is Gaussian [12],

$$a = a_0(r, \xi, \zeta_0) \exp[-2 \ln 2(\xi - \xi_0)^2/(c\tau_L)^2 + i\Psi_0], \quad (1)$$

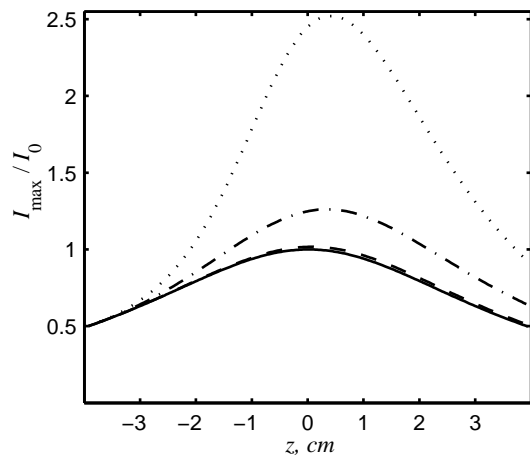


FIG. 1: The maximum intensity of laser pulse on the axis as a function of propagation distance. The vacuum focal plane is $z = 0$. The intensity is normalized to the maximum intensity of laser pulse in the focal plane in vacuum, $I_0 = 6.4 \times 10^{18}$ W/cm². Solid line corresponds to focusing in vacuum; other lines correspond to focusing into plasmas: dashed line — $n_0/n_c = 1.6 \times 10^{-5}$ ($P = P_{cr}$), dash-dotted line — $n_0/n_c = 6.4 \times 10^{-5}$ ($P = 4P_{cr}$), dotted line — $n_0/n_c = 1.28 \times 10^{-4}$ ($P = 8P_{cr}$).

where $\zeta_0 = -z_0/Z_R$, $\Psi_0 = (r/r_0)^2 \zeta_0 / (1 + \zeta_0^2) - \arctan \zeta_0$; $a_0(r, \zeta_0) = a_0(1 + \zeta_0^2)^{-1/2} \exp[-(r/r_0)^2 / (1 + \zeta_0^2)]$; $\xi = \zeta_0$ corresponds to the pulse center; and τ_L is the pulse full width at half-maximum (FWHM) in intensity. At the starting point, the laser pulse (1) has a converging (concave) phase front and focuses into plasma. The simulation proceeds from $z = -Z_R$ to $z = Z_R$, where $Z_R \approx 4$ cm for the parameters chosen. Normalized amplitude of laser in the vacuum focal spot is $a_0 = 1.72$.

A few simulations with different plasma densities demonstrate the effect of nonlinearities on the pulse evolution. The maximum laser intensity on the axis ($r = 0$) is plotted in Fig. 1 versus propagation distance. The density $n_0 = n_{SF} = 2.8 \times 10^{16}$ cm⁻³ gives $P = P_{cr}$ (dashed line). At $n_0 = 8n_{SF}$ (or $P = 8P_{cr}$, dotted line), the non-compensated relativistic self-focusing increases the intensity by a factor of 2.5 in the vicinity of the focal plane. However, for $n_0 = 4n_{SF}$ (or $P = 4P_{cr}$), the on-axis laser intensity varies similarly to the vacuum case (dash-dotted line in Fig. 1). Therefore, under appropriate choice of parameters, propagation of a relativistically strong ultrashort overcritical laser pulse in a rarefied plasma is almost unaffected by the relativistic self-focusing, which could be a challenge for a longer pulse [7].

Figure 2 demonstrates the distortion of the laser radial and temporal profiles due to the decompensation of relativistic self-focusing. For $P \approx 6P_{cr}$, the contour plots of normalized intensity $a^2(\xi, r)$ show that the pulse leading part spreads in the course of propagation, while the trailing part shrinks. The effect manifests in full in the vicinity of the vacuum focal plane. The difference between the speed of light in vacuum and the pulse group

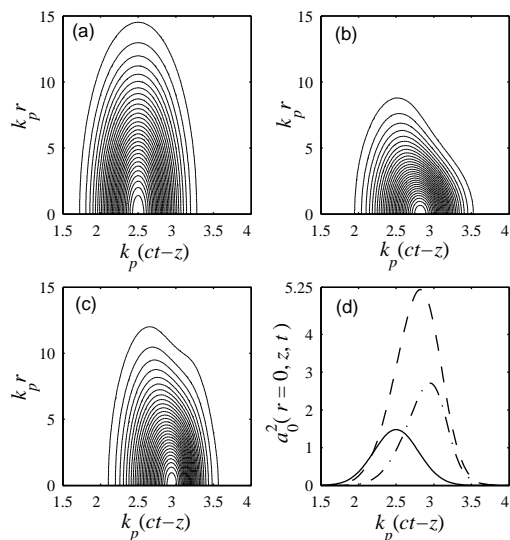


FIG. 2: Contour plots of normalized pulse intensity at the three positions: $z = -Z_R$ (a), $z = 0$ (b), $z = Z_R$ (c). At $z = -Z_R$ the pulse is Gaussian (1) with the amplitude $a_0 = 1.72$, radius $k_p r_0 = 7.84$, and duration $\omega_p \tau_L = 0.68$, which give $P \approx 6P_{cr}$. The solid, dashed and dotted-dashed lines in the plot (d) show the on-axis profile of intensity for the plots (a), (b), and (c).

velocity in plasma brings about the gradually growing shift of the pulse center from its initial position in the co-moving variables.

The analytical consideration given in a weakly relativistic approximation in Appendix A predicts an amplitude threshold a_{0c} [see Eq. (A11)], below which the laser pulse radially spreads according to the linear theory of diffraction for Gaussian beams [12]. For a Gaussian temporal profile, the critical amplitude reads $a_{0c} = (\omega_p \tau_L)^{-1} \sqrt{4 \ln 2 / [1 + (k_p r_0 / 4)^2]}$. The laser amplitude $a_0 = 1.72$ taken in the simulation of Fig. 2 exceeds the critical amplitude $a_{0c} \approx 1.11$, which explains the obvious manifestation of the nonlinearity in Fig. 2. In order to reduce the adverse effect of decompensated nonlinearities, the wakefield evolution and electron acceleration will be further simulated in more rarefied plasmas. The parameters of the case $P = 4P_{cr}$ will be taken, that is, the plasma density $n_0 = 1.12 \times 10^{17}$ cm⁻³ that gives $a_{0c} \approx 1.6$. The relativistic factor of the laser pulse then amounts to $\gamma_g = 125$, and the normalized pulse duration to $\omega_p \tau_L \approx 0.56$.

III. EXCITATION OF NONLINEAR PLASMA WAKEFIELD BY SHORT DIFFRACTING NEARLY GAUSSIAN LASER PULSE

We study numerically and analytically the plasma wakefield evolution in the regime with laser nonlinearities mostly compensated and the laser beam close to Gaussian; the parameters are taken as suggested at the end of

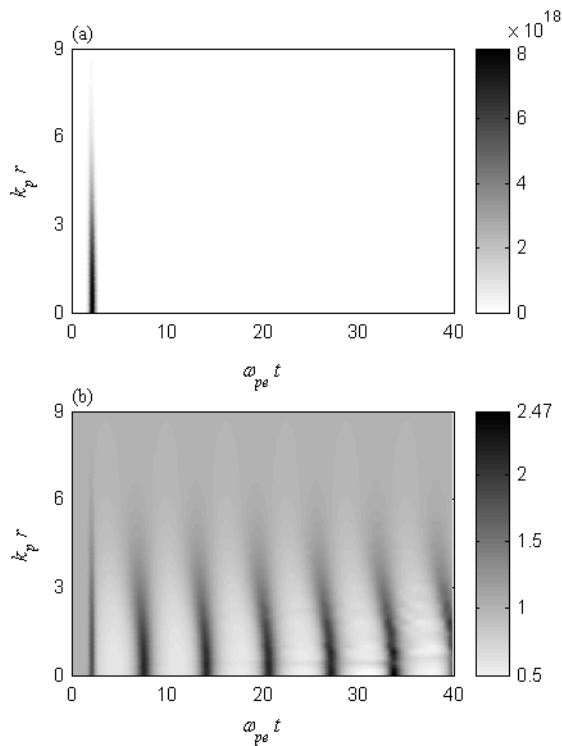


FIG. 3: Temporal evolution of the radial profile of laser pulse intensity (in W/cm^2) (a) and electron density normalized to the background density n_0 (b) in the vacuum focal plane $z = 0$.

section II. Although the laser pulse is much shorter than a plasma period, the intensity on axis is high enough to produce in the wake an electron density perturbation of the order of the background plasma density. The wake becomes strongly nonlinear in the vicinity of focal plane, $z = 0$, where its amplitude is maximal. The radial and temporal profiles of the laser pulse and electron density at this plane are shown in Fig. 3. The wakefield is far from harmonic: the regions of density depression are much wider than the density humps. Moreover, the wake phase front is not plane and its curvature builds up with time. The relativistic shift of plasma frequency in the wake is proportional, to the lowest order, to the laser intensity squared, which radially varies and thus brings about the said curvature [13]. The radial phase variation, however, does not produce a radial wavebreaking [14] within at least six wake periods.

The wake phase velocity is not constant along the laser path. This effect has a purely relativistic origin. As the pulse focuses at $z < 0$, its intensity grows, and so does the relativistic shift of plasma frequency. The wake period stretches, and the phase velocity drops below the group velocity of laser. Beyond the focal plane, $z > 0$, the pulse radially spreads, and the plasma period gradually shrinks thus tending back to the linear limit τ_p . At this stage, the wake phase velocity may exceed both laser pulse group velocity in plasma and the speed of light

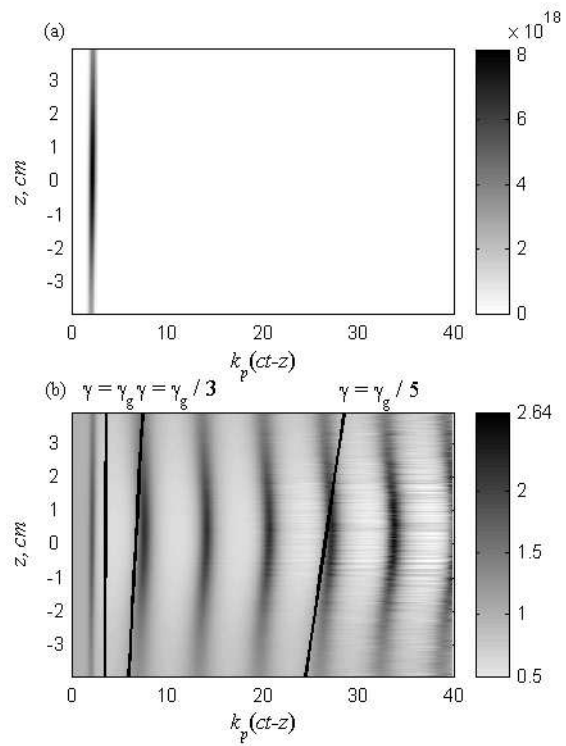


FIG. 4: On-axis evolution of laser intensity (in W/cm^2) (a) and electron density normalized to the background density n_0 (b) as a function of retarded time and laser pulse propagation length in the simulation of Fig. 3. The solid lines in the plot (b) are the tangents to the electron density crests. They characterize the local phase velocity of the wake at $z = z_0 = -Z_R$. Corresponding relativistic factors in units of $\gamma_g = 125$ are shown at the top line of the plot (b).

in vacuum. The luminous point, where the wake phase reaches the vacuum speed of light, does can exist on the path of a laser pulse in a longitudinally inhomogeneous plasma [8]. In our framework, it is due to the nonlinear frequency variation of plasma wake driven by the diffracting laser. Figure 4 shows the on-axis laser intensity (a) and the electron density (b) versus retarded time and distance z in plasma. The plot (b) demonstrates the phase “deceleration” (“acceleration”) at $z < 0$ ($z > 0$) with the wake period stretching (contracting). At $z > 0$ the wake phase is superluminal.

An electron falls in resonance with the accelerating wakefield if its velocity v_{e0} coincides at the point of injection with the local phase velocity of wake. Taking tangents to the electron density crests in Fig. 4(b) helps to evaluate the resonant Lorentz factor $\gamma_{e0} \gg 1$ of the electron injected on axis at $z_0 = -4$ cm. The tangent equation, $z \approx 2\xi\gamma_{e0}^2$, gives $\gamma_{e0} \approx 42 \approx \gamma_g/3$ for the second, and $\gamma_{e0} \approx 21 = \gamma_g/5$ for the fifth wake period. Weakly nonlinear theory of the wakefield excitation by a diffracting short Gaussian laser pulse (see Appendix B) expresses the wake Lorentz factor as a function of normalized pulse position $\zeta = z/Z_R$ and time delay ξ/c [see

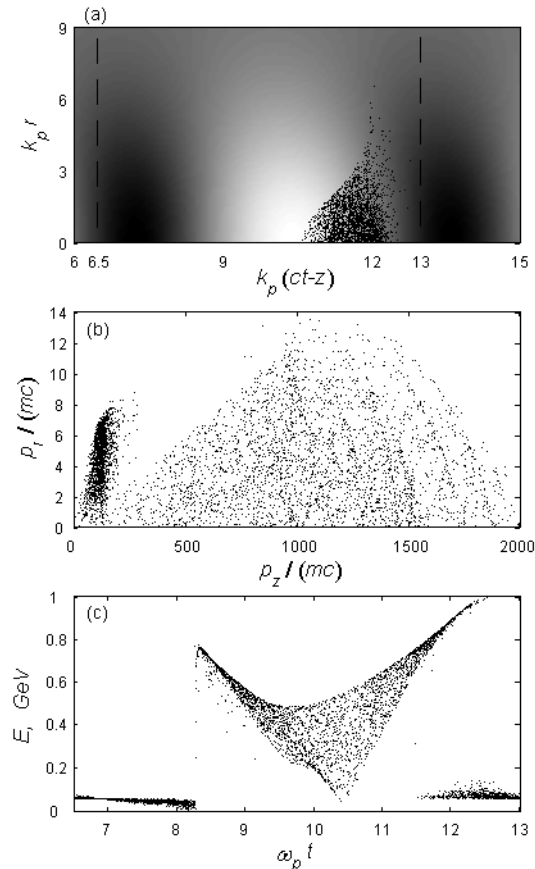


FIG. 5: Acceleration of the resonant electron bunch ($\gamma_{e0} = \gamma_g = 125$). The space distribution (a), momentum distribution (b), and energy versus the injection phase (c) are shown for test electrons crossing the extraction plane $z = Z_R$. Each dot corresponds to a numerical electron. The density of dots characterizes the number of test particles per elementary volume $k_p^2 dr d\xi$ in the plot (a) and per elementary volume of momentum space $(dp_r dp_z)/(mc)^2$ in the plot (b). The grayscale density in the plot (a) is proportional to the normalized wakefield potential $\langle\psi\rangle$, the lightest gray corresponds to $\langle\psi\rangle_{\max} = 0.3$, the darkest gray — to $\langle\psi\rangle_{\min} = -0.24$. Dashed lines in the plot (a) show the boundaries of the bunch at the injection point.

Eq. (B5)], which gives γ_{e0} by a factor of two higher than inferred from the graphical estimates of Fig. 4(b).

IV. ACCELERATION OF RESONANT ELECTRON BUNCHES

The test electron bunch is injected in the laser wake at $z_0 = -Z_R$. At this point, a Monte-Carlo generator creates mono-energetic particles with the energy $mc^2\gamma_{0e}$ and uniform distribution over time interval τ_b . The bunch has a transverse momentum spread, which gives a nonzero initial angular divergence $\langle\alpha^2\rangle^{1/2} = \alpha_e$, and a nonzero initial rms emittance $\varepsilon_{\perp} = (1/2)[\langle r_{\perp}^2\rangle\langle(p_{\perp}/p)^2\rangle - \langle(\mathbf{r}_{\perp} \cdot$

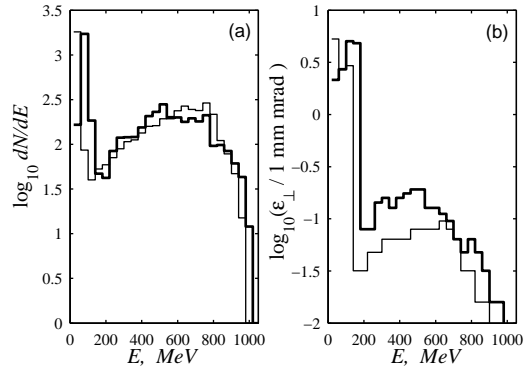


FIG. 6: Energy spectrum (a) and emittance (b) at the extraction plane $z = Z_R$ for electron bunches injected with $\gamma_{e0} = 125$ (thick lines) and $\gamma_{e0} = 42$ (thin lines) into the second wake period.

$\mathbf{p}_{\perp})/p)^2]^{1/2}$ (Ref. 15). Radial distribution of electron density in the bunch is Gaussian with an rms radius $\sigma \sim r_0$. The accelerated electrons are extracted from the wake at $z = Z_R$.

First, the conventional resonant condition $\gamma_{e0} = \gamma_g$ is considered. A bunch of 5000 test electrons with $\gamma_{e0} = 125$, zero angular divergence, and $k_p\sigma = k_p r_0/\sqrt{2} = 4.5$ is accelerated in the second wake period ($6.5 \leq k_p\xi \leq 13$, which corresponds to the bunch duration $\tau_b \approx 330$ fs). Distributions of test electrons in coordinate and momentum space at $z = Z_R$, and final energy versus injection phase are shown in Fig. 5. The grayscale background in the plot (a) is the normalized potential $\langle\psi\rangle = [e/(mc^2)]\langle A_z - \Phi\rangle$, where $\langle\cdots\rangle$ means the averaging over the laser period $2\pi/\omega_0$, $\langle A_z\rangle$ and $\langle\Phi\rangle$ are vector and scalar potentials associated with low-frequency wakefields. This potential determines the low-frequency electric and magnetic fields in plasma, and, hence, the forces acting on test electrons. The plot (a) shows that accelerated particles are collected in the focusing and accelerating quarter of the wakefield period. Quite a few electrons stay near the bottom of the potential well with the energy gain, as is testified by the plot (c), almost negligible. The transverse spread of the bunch is reduced roughly twice if compared with the initial value.

Figure 6 shows the final energy and emittance of the test electrons collected by equally distributed channels of an electron spectrometer. We compare them for the two different resonant condition fulfilled at the injection plane. The thick lines correspond to $\gamma_{e0} = \gamma_g = 125$ (resonance with the laser pulse) and the thin ones to $\gamma_{e0} = \gamma_{p0} \approx 42$. This value of γ_{e0} corresponds to the resonance with the second period of the plasma wake when the injection point is on the axis. In both cases the energy spectrum looks as a shoulder with not too pronounced maxima near 0.5 GeV for $\gamma_{e0} = 125$ and 0.75 GeV for $\gamma_{e0} = 42$. There is no explicit energy gap separating the accelerated electrons from those which are non-accelerated. In the case of $\gamma_{e0} = 42$ the final emi-

tance is smaller than that for $\gamma_{e0} = 125$ [see the plot (b)]. The energy cutoff appears to be independent of the injected electron energy and is close to 1 GeV.

The energy limit of 1 GeV can be exceeded if the electrons are injected earlier and extracted from the wake later. Additional runs show that elongating the acceleration length by 50% ($-1.5Z_R \leq z \leq 1.5Z_R$) gives a 15% increase in the maximum of final energy. As the highest acceleration gradients are achieved near the laser focus, increasing the acceleration length beyond $2Z_R$ does not lead to a substantial growth of electron energy.

Analysis of Figs. 5 and 6 leads to the following conclusion: injection of a quite long (of the order of or longer than a wake period) resonant electron bunch results in a large energy spread of trapped and accelerated electrons no matter whether the injected bunch was resonant with the laser pulse or with a given period of the wake. It is obvious that the resonant conditions $\gamma_{e0} = \gamma_g$ or $\gamma_{e0} = \gamma_{p0}$ serve well only for the electrons injected in just one quarter (focusing and accelerating) of the wake period. Sample simulation made for a short electron bunch ($11.5 \leq k_p \xi \leq 12.5$) with $\gamma_{e0} = 125$ and zero initial emittance gave the mean output 0.85 GeV per electron with about 30% energy spread.

V. ACCELERATION OF NON-RESONANT ELECTRON BUNCHES

Now studying non-resonant injected electron bunches, we bear in mind that the initial energy of electrons is essentially smaller than that of the resonant ones. Figure 7 presents the same plots as Fig. 5 but for injected electrons with $\gamma_{e0} = 10 \ll \gamma_{g(p0)}$.

Comparison of Figs. 5 and 7 reveals certain benefits of using the electrons non-resonant at injection. First, the accelerated bunch of initially non-resonant particles is more compact in the radial direction [compare plots (a) of the two figures], and the radial momentum spread is lower [compare plots (b)]. Fig. 7(a) shows no electrons at the bottom of the potential well, $k_p \xi \approx 10$, hence, all the trapped non-resonant electrons are accelerated, and the energy gap finally appears between the trapped and non-trapped particles [see Fig. 7(c)]. Opposite to the resonant case, the non-resonant electrons, loaded into either accelerating or decelerating focusing phases, gain almost the same energy. At the point of injection, the wake phase outruns the non-resonant particles, so they slip out of the disadvantageous phase towards the focusing and accelerating one. Otherwise, the resonant electrons are initially at rest in the decelerating phase, and their slippage takes more time. So, their final energy proves to be lower.

Figure 8 shows final energy spectrum and emittance of initially non-resonant test electrons with $\gamma_{e0} = 10$, injected at $z_0 = -Z_R$ with zero initial emittance in the second ($6.5 \leq k_p \xi \leq 13$, simulation of Fig. 7) and sixth ($32.1 \leq k_p \xi \leq 38.4$) wake periods. The initial rms radius of the bunch is the same as in Figs. 5 and 7. The electrons

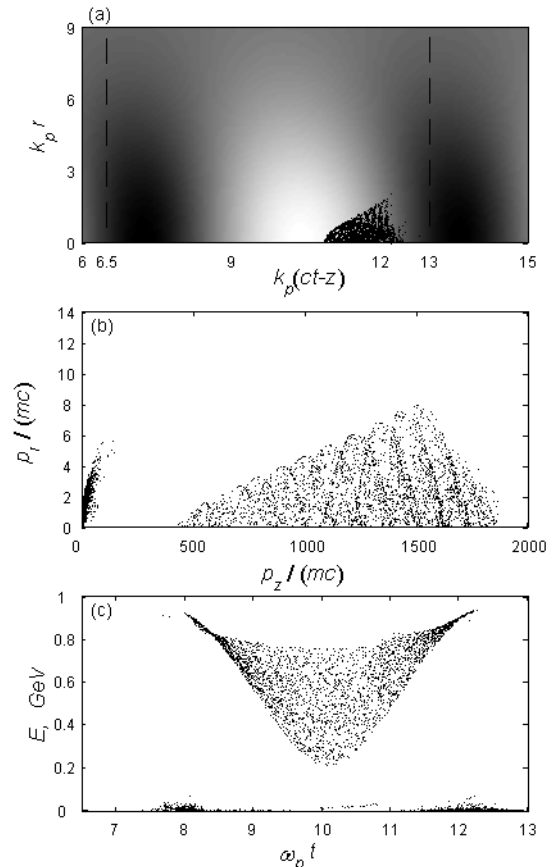


FIG. 7: Acceleration of the non-resonant electron bunch. All parameters being the same as in Fig. 5, except of initial relativistic factor of electrons $\gamma_{e0} = 10 \ll \gamma_g$.

accelerated in the second wake period are separated from the bulk of low energetic particles by a 150 MeV wide gap [see also Fig. 7(c)]. Besides, efficiency of acceleration reduces when the time delay between the laser pulse and electron bunch grows. The spectrum of electrons accelerated in the second period has the maximum at 0.8 GeV and a sharp cutoff at 0.95 GeV. Acceleration in the sixth period gives a plateau-like energy spectrum which rises steadily up to 0.65 GeV and drops at 0.85 GeV. Therefore, the injection time lag should be taken as small as possible in order to reduce the adverse effect of the wake phase velocity variation. As compared with the resonant case [Fig. 6(b)], final emittance of the bunch is typically lower in the non-resonant case (by a factor of three for the spectrometer bins beyond 500 MeV).

Technological limitations of monoenergetic electron injectors lead inevitably to using in the experiment long ($\tau_b \gg \tau_p$) and wide ($k_p \sigma \gg 2\pi$) electron bunches with nonzero rms emittance. The results of sample modelling of this situation are presented in Fig. 9. The energy spectrum (a) and rms emittance (b) of accelerated electrons are shown at the extraction point $z = Z_R$. The non-resonant ($\gamma_{e0} = 10$) electron beam injected at $z_0 = -Z_R$

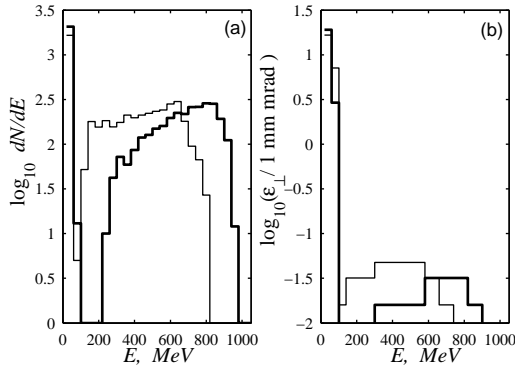


FIG. 8: Final energy spectrum (a) and emittance (b) of electrons injected in different wake periods. The electron are injected with $\gamma_{e0} = 10$. Thick and thin lines correspond to the injection to the second (data from simulation of Fig. 7) and sixth period, respectively.

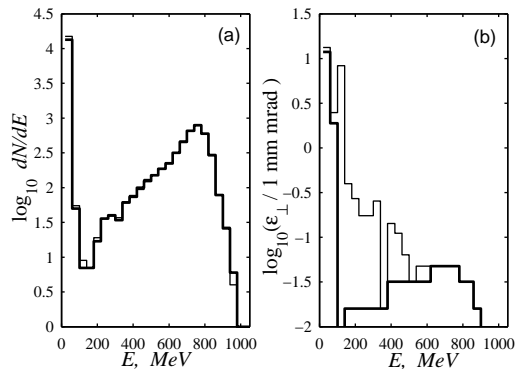


FIG. 9: Energy spectrum (a) and rms emittance (b) of accelerated electrons for non-resonant ($\gamma_{e0} = 10$) wide ($k_p\sigma = 13.5$) and long ($6.5 \leq k_p\xi \leq 25.4$) electron bunch with zero initial emittance (thick lines) and with an initial rms emittance $\varepsilon_{\perp} = 2.145$ mm mrad (thin lines).

covers three consecutive wake periods, $6.5 \leq k_p\xi \leq 25.4$. The transverse size of the beam $k_p\sigma = 13.5$ is by a factor of three larger than that of Figs. 5 and 7, and the number of particles in the bunch is 20000. The thick lines correspond to the bunch with zero rms emittance at injection, and the thin lines to the case with initial rms emittance $\varepsilon_{\perp} = 2.145$ mm mrad. Variation of the initial rms emittance has a negligible effect on the energy spectrum which has a sharp maximum at 0.75 GeV and cut-off at 0.95 GeV. Only emittance of low-energy electrons (spectrometer bins at $E < 500$ MeV) is increased due to nonzero rms emittance of the injected beam. The emittance of the higher-energy electrons is unaffected. Thus, the simulations show that elongating the electron bunch still preserves all the benefits of using the non-resonant electrons and does not create any challenge for the experimental implementation of the proposed scheme.

Effective trapping and acceleration of electrons also occurs for bunches injected with very low energy ($E_{in} \sim$

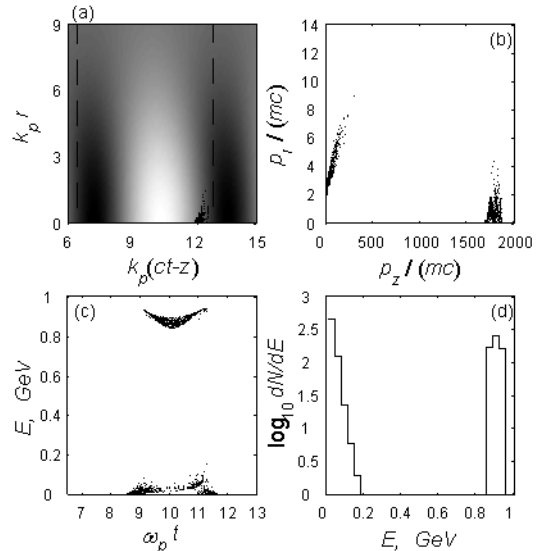


FIG. 10: Acceleration of low-energy electron bunch ($\gamma_{e0} = 2$). Plots (a)-(c) show the same quantities as in Figs. 5 and 7. The electron energy spectrum is shown in plot (d). Injection of highly non-resonant bunch provides almost monoenergetic acceleration of trapped electrons.

1 MeV), which lead to almost monoenergetic acceleration [16]. In Fig. 10, the energy spectrum of accelerated electrons with initial relativistic factor $\gamma_{e0} = 2$ and radial spread $k_p\sigma = 2$ is shown while the other parameters are taken the same as of Figs. 5 and 7. The total number of injected particles is 2500, of which roughly one half is trapped and accelerated up to 900 MeV with 10% energy spread. The final rms emittance of accelerated bunch is lower than 10^{-4} mm mrad.

VI. CONCLUSION

Construction of the petawatt ultra-short-pulse lasers will create an opportunity for standard LWFA of electrons up to GeV energies. In quite tenuous plasmas ($\omega_p < \tau_L^{-1}$) the relativistic and ponderomotive nonlinearities of a not very tightly focused ($k_p r_0 \geq 2\pi$) laser pulse cancel each other [9]. In this regime, an overcritical laser pulse propagates like in vacuum. Increasing the laser focal spot up to 100 μm in radius elongates the laser-plasma interaction length (estimated as twice the Rayleigh length) up to 8 cm without any external optical guiding. Such not very tightly focused laser pulse, however, has enough energy to drive a nonlinear plasma wakefield along this distance, which provides a controllable acceleration of externally injected electrons up to 1 GeV. The nonlinear features of quasi-plane wave plasma wave facilitate trapping, focusing, and acceleration of the electrons from the injected bunch. The converging laser pulse drives the plasma wake whose period stretches (due

to relativistic decrease in plasma frequency) as the pulse approaches the focal plane. At this stage, the wake phase velocity drops below the pulse group velocity. Growth of the wake amplitude combined with the decrease in the phase velocity provides the efficient trapping of low-energy (non-resonant) electrons. Beyond the focal plane, the laser pulse diverges, and the wake phase may become superluminal, which makes for additional longitudinal compression of the electron bunch in the focusing and accelerating quarter of the wakefield period. These features of wakefield structure reduce the energy spread and emittance of the electron bunch injected out of resonance with the wake, $\gamma_{e0} \ll \gamma_{g(p0)}$, and, in the limit of very low initial energy (1 MeV), provide almost monoenergetic acceleration.

Acknowledgments

L. M. G. and S. Yu. K. gratefully acknowledge the hospitality of CPhT, École Polytechnique. This work was partly supported by Centre National de la Recherche Scientifique (France) in the frame of cooperation with the Russian Academy of Sciences, the École Polytechnique (in the form of postdoctoral fellowship for S. Yu. K.), the Russian Fund for Basic Research (Grant No. 02-02-1611), and by the U.S. Dept. of Energy under Contracts No. DE-FG02-04ER54763 and DE-FG02-04ER41321.

APPENDIX A: NONLINEAR EFFECTS IN PROPAGATION OF ULTRA-SHORT LASER PULSES

Self-consistent evolution of axi-symmetric laser pulse and perturbations of electron plasma density can be described in the weakly nonlinear quasi-static approximation by the set of equations [17],

$$2ik_0 \frac{\partial a}{\partial z} + \Delta_{\perp} a = k_p^2 \left(N - \frac{1}{4}|a|^2 \right) a, \quad (\text{A1a})$$

$$\frac{\partial^2 N}{\partial \xi^2} + k_p^2 N = \frac{1}{4} \left(\frac{\partial^2}{\partial \xi^2} + \Delta_{\perp} \right) |a|^2, \quad (\text{A1b})$$

where $a = eE/(m\omega_0 c)$ is the normalized amplitude of the laser electric field, $N \equiv (n_e - n_0)/n_0$ is the normalized electron density perturbation, and $\Delta_{\perp} \equiv r^{-1} \partial / \partial r (r \partial / \partial r)$ is the radial part of the Laplace operator.

In the limit of a short and wide pulse whose length $c\tau_L$ is smaller but the radius r_0 is larger than k_p^{-1} , the main terms in Eq. (A1b) are those containing the second derivatives with respect to ξ . In this approximation, the nonlinear terms in the right-hand side (RHS) of Eq. (A1a) cancel each other, and the pulse propagates as in vacuum [9]. The small corrections to the index of refraction which are due to the finite pulse length and proportional to $(\omega_p \tau_L)^2$ were considered in Ref. 9. We

consider the effect of small longitudinal and transverse nonlinearities on the evolution of a short laser pulse and assume the transverse pulse shape be Gaussian in every cross-section,

$$a = \frac{A_0(\xi)}{f(\xi, z)} \exp \left[-\frac{r^2}{r_0^2 f^2} + i \left(\frac{r^2}{2} \beta(\xi, z) + \varphi(\xi, z) \right) \right]. \quad (\text{A2})$$

Here, $f(\xi, z)$ is the dimensionless focal spot size (pulse width) which equals unity in the focal plane $z = 0$ [i.e., $f(\xi, 0) \equiv 1$]. The function $A_0(\xi)$ gives an initial amplitude profile on axis, the initial focal spot radius is r_0 , the quantities $\varphi(\xi, z)$ and $\beta(\xi, z)$ give the on-axis values of phase and curvature of the laser phase front, respectively. Substituting Eq. (A2) into Eqs. (A1) gives the equation for the pulse width [18],

$$\frac{\partial^2 f}{\partial z^2} - \frac{f^{-3}}{Z_R^2} = -\frac{f \omega_p k_p^3}{4 \omega_0 Z_R} \times \int_{-\infty}^{\xi} d\xi' \sin[k_p(\xi - \xi')] \frac{A_0^2(\xi')}{f^4(\xi', z)} \left(1 + \frac{16}{k_p^2 r_0^2 f^2(\xi', z)} \right), \quad (\text{A3})$$

where z is the coordinate of the pulse center moving from the left to the right; the transverse Laplace operator in Eq. (A1b) gives the second term in the brackets in the integrand. In the short-pulse case, $A_0^2(\xi)$ is nonzero within an interval $|\xi| \ll k_p^{-1}$. Integrating by parts the expression in the RHS of Eq. (A3) and taking account of only the main term gives

$$\frac{\partial^2 f}{\partial z^2} - \frac{f^{-3}}{Z_R^2} = -\frac{f \omega_p k_p^3}{4 \omega_0 Z_R} \times \int_{-\infty}^{\xi} d\xi' \int_{-\infty}^{\xi'} d\xi'' \frac{A_0^2(\xi'')}{f^4(\xi'', z)} \left(1 + \frac{16}{k_p^2 r_0^2 f^2(\xi'', z)} \right). \quad (\text{A4})$$

The laser pulse of small amplitude propagates in plasma as in vacuum. In order to evaluate the threshold amplitude a_{0c} above which the effect of nonlinearities might occur, we consider Eq. (A4) near the focal plane. At the focal plane $z = 0$ the pulse width f is constant while $A_0(\xi)$ alters within a relatively short interval $|\xi| \ll k_p^{-1}$. We assume that $f(\xi, z)$ varies with ξ slower than $A_0(\xi)$ within some segment of the laser path. Equation (A4) then reduces to

$$\frac{\partial^2 f}{\partial \zeta^2} - \frac{1}{f^3} \left\{ 1 - \alpha I(\xi) \left(1 + \frac{2}{\alpha f^2} \right) \right\} = 0, \quad (\text{A5})$$

where $\zeta = z/Z_R$ is the normalized propagation distance, $\alpha = (k_p r_0)^2/8$ is the normalized initial squared spot size

$$I(\xi) = k_p^2 \int_{-\infty}^{\xi} d\xi' \int_{-\infty}^{\xi'} d\xi'' A_0^2(\xi''). \quad (\text{A6})$$

The condition $f(\xi, 0) \equiv 1$ gives the integral of Eq. (A5),

$$\left(\frac{\partial f}{\partial \zeta} \right)^2 - \left(1 - \frac{1}{f^2} \right) \left[1 - \alpha I - I \left(1 + \frac{1}{f^2} \right) \right] = 0. \quad (\text{A7})$$

Initially, the evolution of a small spot size perturbation $\delta f = f - 1$, $|\delta f| < 1$, obey the equation following from Eq. (A7),

$$(\partial\delta f/\partial q)^2 - 2\delta f(B - 1) = 0, \quad (\text{A8})$$

where $q = \zeta\sqrt{I}$, and $B = I^{-1} - 1 - \alpha$. Equation (A8) has real solutions for both $B < 1$ (then $\delta f < 0$) and $B > 1$ (then $\delta f > 0$). Reduction of the pulse width in the first case corresponds to the converging laser pulse, while in the second case the laser diverges. The border of laser pulse stability against the transverse distortions, $B = 1$, gives the implicit equation for the stability point,

$$I(\xi_c) = (2 + \alpha)^{-1}. \quad (\text{A9})$$

The point ξ_c separates diverging and converging parts in the pulse profile. The function $I(\xi)$ grows monotonically from the leading front towards the trailing edge of the pulse. Therefore, the pulse portion which lays between the leading front and the point ξ_c spreads, while the part beyond ξ_c focuses. As a result, in the process of propagation the short pulse acquires the form similar to "beet-root". In the vicinity of the threshold point ξ_c , the pulse width given by Eq. (A8) reads $f = 1 - (\zeta^2/2)[I(\xi) - I(\xi_c)]/I(\xi_c)$.

We examine the case of a Gaussian laser pulse, $A_0(\xi) = a_0 \exp[-2 \ln 2 \xi^2 / (c\tau_L)^2]$, with the center located at $\xi = 0$. Substituting $A_0(\xi)$ into Eq. (A6) gives

$$I(\xi) = \frac{(a_0\omega_p\tau_L)^2}{8 \ln 2} \int_{-\xi\sqrt{2 \ln 2} / (c\tau_L)}^{\infty} dx [1 - \Phi(x)], \quad (\text{A10})$$

where

$$\Phi(x) = \frac{2}{\sqrt{\pi}} \int_0^x dt \exp(-t^2)$$

is the probability integral. Substantial modification of the laser pulse shape occurs when the threshold condition (A10) is met at the pulse center (i.e., $\xi_c = 0$). In consistence with Eq. (A10), this criterion takes the form

$$a_{0c} = \frac{1}{\omega_p\tau_L} \sqrt{\frac{4 \ln 2}{1 + (k_p r_0/4)^2}}. \quad (\text{A11})$$

APPENDIX B: THE WAKEFIELD OF AN ULTRA-SHORT FOCUSING LASER PULSE

The wakefield is excited by the ponderomotive force associated with a laser pulse. Under the assumption that the linear theory of diffraction of Gaussian beams [12] holds, the laser pulse envelope $a(r, z, \xi)$ reads

$$a = \frac{a_0}{\sqrt{1 + \zeta^2}} \exp \left[-2 \ln 2 \frac{\xi^2}{(c\tau_L)^2} - \frac{r^2}{r_0^2(1 + \zeta^2)} + i\Psi \right], \quad (\text{B1})$$

where $\zeta = z/Z_R$, $\xi = v_g t - (z + z_0)$, $\Psi = (r/r_0)^2 \zeta / (1 + \zeta^2) - \arctan \zeta$, v_g is the group velocity of a pulse, other

notations are the same as in Eq. (1). At the initial moment $t = 0$, the pulse center $\xi = 0$ resides at $z = -z_0$. The pulse propagates towards positive z .

In the linear approximation, the frequency of electron plasma oscillation equals ω_p , and the phase velocity v_p of the wake coincides with the group velocity v_g of the pulse. In the weakly nonlinear approximation, the frequency of plasma oscillations is downshifted because of relativistic increase of the mass of oscillating electron [19]. The intensity of the Gaussian beam (B1) varies along the laser path, and so does the amplitude of the plasma wake. Hence, relativistic reduction of the plasma frequency alters as a function of propagation distance, and this phase slippage characterizes the variation of the phase velocity of the wake across the plasma. Consideration of this effect is easier in the case of a wide, $k_p r_0 \gg 1$, and not so intense, $a_0 < 1$, laser pulse when the wake electric field is the potential one. Then, for the laser pulse amplitude taken in the form (B1), the dimensionless wake potential $\phi = e\varphi/(mc^2)$ is given by [3]

$$\phi = -\frac{(a_0/2)^2 g(x)}{1 + \zeta^2} \times \exp \left[-\frac{2r^2}{r_0^2(1 + \zeta^2)} \right] \sin \left\{ \left[k_p + \frac{\Delta\omega_p(z, r)}{c} \right] \xi \right\}, \quad (\text{B2})$$

where $g(x) = x\sqrt{\pi/2} \exp(-x^2/8)$ depends on the dimensionless pulse length $x = \omega_p\tau_L/\sqrt{2 \ln 2}$, the relativistic frequency shift [19] is $\Delta\omega_p = -(3/16)\omega_p[(a_0/2)^2/(1 + \zeta^2)]^2 \exp[-(2r/r_0)^2/(1 + \zeta^2)]g^2(x)$. The on-axis phase of the wake potential follows from Eq. (B2),

$$\theta = k_p(v_g t - z) \left\{ 1 - \frac{3}{16} \left[\frac{(a_0/2)^2 g(x)}{1 + \zeta^2} \right]^2 \right\}. \quad (\text{B3})$$

Then, the wake phase velocity v_p reads

$$v_p = -\frac{\partial\theta/\partial t}{\partial\theta/\partial z} \approx v_g \left\{ 1 + \frac{3}{4} \left[\frac{(a_0/2)^2 g(x)}{1 + \zeta^2} \right]^2 \frac{\zeta\xi/Z_R}{1 + \zeta^2} \right\}. \quad (\text{B4})$$

The quantity ξ/v_g characterizes a positive time delay with respect to the pulse center, and ζ characterizes the laser pulse position relative to the focal plane. When the pulse passes the focal plane, ζ becomes positive. The wake phase velocity coincides with the pulse group velocity only far away from the focal plane and exactly at the focal plane. The wake phase velocity decreases while the pulse approaches the focal plane, and reaches the minimum value for $z = -Z_R/\sqrt{5}$ where $v_p \approx v_g \{1 - 0.192[(a_0/2)^2 g(x)]^2 \xi/Z_R\}$. The wake phase velocity exceeds v_g and can exceed the vacuum speed of light while the pulse moves away from the focal plane and radially spreads. Small variation of the phase velocity v_p with respect to v_g can, however, considerably modify the Lorentz factor $\gamma_{p0} \equiv (1 - v_p^2/c^2)^{-1/2}$ if compared with $\gamma_g \equiv (1 - v_g^2/c^2)^{-1/2}$. Eq. (B4) gives

$$\gamma_{p0}^{-2} \approx \gamma_g^{-2} + \frac{3}{2} \left[\frac{(a_0/2)^2 g(x)}{1 + \zeta^2} \right]^2 \frac{\zeta\xi/Z_R}{1 + \zeta^2}. \quad (\text{B5})$$

The electrons are injected at negative ζ where $v_p < v_g$. Hence, the resonance with the nonlinear wakefield needs less electron energy ($mc^2\gamma_{p0}$) than the resonance with the laser pulse (or a linear wakefield), $mc^2\gamma_g$.

Although Eq. (B5) is weakly relativistic, we use it for a qualitative estimate of resonant gamma-factors for different wake periods for the simulation parameters of Sec. IV and V ($\omega_p\tau_L = 0.56$, $a_0 = 1.72$, $k_p r_0 = 6.3$,

$Z_R = 4$ cm, $\gamma_g = 125$). The accelerating phase of the second period (See Fig. 5) corresponds to $k_p\xi \approx 6.5$ (i.e., $\xi = -0.01$ cm), and, at the point of injection $\zeta = -1$, has a gamma-factor $\gamma_{p0} \approx 80$. For the accelerating phase of the fifth plasma period ($k_p\xi \approx 25$) Eq. (B5) gives $\gamma_{p0} \approx 49$. Graphic estimates of resonant Lorentz factors in Fig. 4(b) exceed the weakly relativistic estimates roughly by a factor two.

-
- [1] T. Tajima and J. M. Dawson, Phys. Rev. Lett. **43**, 267 (1979).
- [2] E. Esarey, P. Sprangle, J. Krall, and A. Ting, IEEE Trans. Plasma Sci. **PS-24**, 252 (1996).
- [3] F. Amiranoff, S. Baton, D. Bernard, *et al.*, Phys. Rev. Lett. **81**, 995 (1998); F. Dorchies, F. Amiranoff, V. Malka *et al.*, Phys. Plasmas **6**, 2903 (1999).
- [4] M. Aoyama, K. Yamakawa, Y. Akahane, J. Ma, N. Inoue, H. Ueda, and H. Kiriya, Opt. Lett. **28**, 1594 (2003).
- [5] T. M. Antonsen Jr. and P. Mora, Phys. Rev. Lett. **69**, 2204 (1992); Phys. Fluids B **5**, 1440 (1993).
- [6] P. Mora and T. M. Antonsen Jr., Phys. Rev. E **53**, R2068 (1996); Phys. Plasmas **4**, 217 (1997).
- [7] A. G. Litvak, Sov. Phys. JETP **30**, 344 (1969); G.-Z. Sun, E. Ott, Y. C. Lee, and P. Guzdar, Phys. Fluids **30**, 526 (1987).
- [8] T. Katsouleas, Phys. Rev. A **33**, 2056 (1986); P. Sprangle, B. Hafizi, J. R. Peñano, R. F. Hubbard, A. Ting, A. Zigler, and T. M. Antonsen, Jr., Phys. Rev. Lett. **85**, 5110 (2000); P. Sprangle, B. Hafizi, J. R. Peñano *et al.*, Phys. Rev. E **63**, 056405 (2001).
- [9] P. Sprangle, E. Esarey, and A. Ting, Phys. Rev. Lett. **64**, 2011 (1990); Phys. Rev. A **41**, 4463, (1990).
- [10] J. Faure, V. Malka, J.-R. Marquès, P.-G. David, F. Amiranoff, K. Ta Phuoc and A. Rousse, Phys. Plasmas **9**, 756 (2002); C. Delfin, V. Lokhnygin, J. Mauritsson, A. Sjögren, C.-G. Wahlström, A. Pukhov and G. D. Tsakiris, *ibid.* **9**, 937 (2002).
- [11] J.-R. Marquès, F. Dorchies, F. Amiranoff *et al.*, Phys. Plasmas **5**, 1162 (1998).
- [12] Joseph T. Verdeyen, *Laser Electronics* (Prentice-Hall, Inc., Englewood Cliffs, N. J. 07632, 1981), p. 53.
- [13] C. D. Decker, W. B. Mori, and T. Katsouleas, Phys. Rev. E **50**, R3338 (1994); S. V. Bulanov, F. Pegoraro, and A. M. Pukhov, Phys. Rev. Lett. **74**, 710 (1995); N. E. Andreev, L. M. Gorbunov, and R. R. Ramazashvili, Plasma Phys. Rep. **23**, 277 (1997).
- [14] S. V. Bulanov, F. Pegoraro, A. M. Pukhov, and A. S. Sakharov, Phys. Rev. Lett. **78**, 4205 (1997);
- [15] P. Mora, J. Appl. Phys. **71**, 2087 (1992).
- [16] R. F. Hubbard, D. F. Gordon, A. Ting *et al.*, Bull. Am. Soc. **48**, 106 (2003).
- [17] N. E. Andreev, L. M. Gorbunov, V. I. Kirsanov, A. A. Pogosova, and R. R. Ramazashvili, JETP Lett. **55**, 571 (1992).
- [18] N. E. Andreev, V. I. Kirsanov, and L. M. Gorbunov, Phys. Plasmas **2**, 2573 (1995).
- [19] M. N. Rosenbluth and C.S.Liu, Phys. Rev. Lett. **29**, 701 (1972); C. J. McKinstrie and D. W. Forslund, Phys. Fluids **30**, 904 (1987)